Supplementary Information (SI) for Journal of Materials Chemistry A.
This journal is © The Royal Society of Chemistry 2026

Taming *OH intermediates via deficient engineering to suppress oxygen evolution for efficient glycerol electrooxidation coupled hydrogen production

Zhi-Yuan Feng[1], Jing Wang[2 **], Long-Yue Meng[1*]

[1] Department of Chemistry, College of Science, Yanbian University, Yanji, 133002, PR China

[2] Hebei Key Laboratory of Heavy Metal Deep-Remediation in Water and Resource Reuse, Yanshan University, Qinhuangdao, Hebei 066004, China

[3] Laboratory of Catalysis for Energy and Resources, Yanbian University; Jilin Province Key Laboratory of Catalysis for Green and Low Carbon Energy and Resources, Yanji, Jilin Province, 133002, P. R. China

Author Contact Information:

* Corresponding author. E-mail address: lymeng@ybu.edu.cn.

** Co-corresponding author. E-mail address: jwang6027@ysu.edu.cn.

Method

Synthesis of Dy-$NiMoO_4$/NF

Nickel foam (NF) was cut to the size of 1*2 cm and ultrasounded in 1 M HCl, acetone and ethanol for 15 min. To prepare $NiMoO_4$, 40 mM nickel nitrate hexahydrate [$Ni(NO_3)_2 \cdot 6H_2O$], 10 mmol ammonium molybdate [$(NH_4)_6Mo_7O_{24} \cdot 4H_2O$] and dysprosium nitrate hexahydrate [$Dy(NO_3)_2 \cdot 6H_2O$] were dissolved in 50mL deionized water. After stirring for 30 min, the treated NF was transferred to a 50 mL Teflon-lined autoclave and kept at 150℃ for 6 h. After cooling to room temperature, the sample was rinsed with deionized water and ethanol for 3 times, and dried in an oven at 80℃ for 10 h. The obtained sample was recorded as Dy-$NiMoO_4$/NF.

Synthesis of Sv/Dy-$NiMoO_4$/NF

0.3g sulfur powder was measured and placed in the upper reaches of the tube furnace, Dy-$NiMoO_4$/NF was placed in a corundum boat and placed in the lower reaches of the tube furnace, and heated at 300 ℃ for 2 h in N_2 atmosphere with the heating rate of 5 ℃ min−1, The obtained sample is denoted as S/Dy-$NiMoO_4$/NF. In order to construct sulfur vacancy, S/Dy-$NiMoO_4$/NF was put into the plasma chamber for 2.5, 5, 7.5 and 10 min respectively in Ar atmosphere with power of 100 W, and the obtained sample was recorded as Sv/Dy-$NiMoO_4$/NF.

Materials characterization

The morphological and structural features of Sv/Dy-$NiMoO_4$/NF were characterized using scanning electron microscopy (SEM; Thermo Scientific Apreo 2S) and transmission electron microscopy (TEM; Talos F200S). The lattice structure of the samples was characterized using powder X-ray diffraction (XRD, Rigaku Ultima IV). The elemental compounds were analyzed using X-ray photoelectron spectroscopy (XPS, Thermo Fischer, ESCALAB 250Xi). S/Dy-$NiMoO_4$/NF and Sv/Dy-$NiMoO_4$/NF were analyzed using a micro-confocal Raman spectrometer (Thermo Scientific Dxr2xi). The water and oxygen contact angles of Sv/Dy-$NiMoO_4$/NF were determined using a contact angle-measuring device (JY-82C). The work function was obtained by ultraviolet photoelectron spectroscopy (UPS, Thermo Scientific NEXSA): A He discharge lamp with the He (I) photoline (21.22 eV) was applied, and the high-binding

energy secondary electron cutoff (Ecutoff) and the energy gap (ΔE) between the valence band maximum (VBM) and the fermi level were extracted from the UPS spectra. The data were acquired with -5 V bias. The work function was calculated as Equation:

$$\text{work function} = 21.22 - \text{Ecutoff}$$

^{1}H nuclear magnetic resonance (NMR) spectra were obtained using a superconducting magnet NMR spectrometer (Bruker AVANCE III HD 500 MHz).

Electrochemical measurements

All electrochemical tests were performed with a three-electrode system by a CHI-760E, the prepared electrocatalyst was used as the working electrode, the Hg/HgO electrode (1.0 M potassium hydroxide) as the reference electrode and the graphite rod as the counter electrode. All of the potentials involved were based on the reversible hydrogen electrode (RHE): $E_{RHE} = E_{Hg/HgO} + 0.059\ pH + 0.098$. The electrochemical properties evaluation of all prepared electrodes were performed in 1.0 M KOH, 1.0 M KOH+ 0.1 M glycerol for HER, OER and glycerol electrooxidation characterization with iR compensation. The electrochemical double layer capacitance (C_{dl}) was determined by cyclic voltammetry (CV) curves at different scan rates from 10 to 50 mV s^{-1}. EIS measurements were carried out in the frequency range from 0.1 Hz to 100 kHz with an amplitude of 5 mV. The stability of Sv/Dy-$NiMoO_4$/NF in different solutions was tested by chronoamperometric i-t measurement. To quantify the concentration of formate generated in the electrolysis, glycerol electrolyte (0.1 mL) and a deuterium oxide (D_2O) solution (0.5 mL) containing 5 mg mL^{-1} maleic acid (internal standard) were mixed. The Faraday efficiency (FE) and formate productivity were determined using the following equation:

$$FE_{H2} = m*n*F/It*100\%$$

$$FE_{formate} = nFcV/Q$$

where c is the molar concentrations of formate, n is the number of electrons transferred, V is the electrolyte volume, F is the Faraday constant (96485 C mol^{-1}), and Q is the total charge during electrolysis.The conversion of glycerol were determined

using the following equation:

$$\text{Conversion (\%)} = [C_i(\text{glycerol}) - C_f(\text{glycerol}))/C_i(\text{glycerol})] \times 100\%$$

where C_i is initial concentration and C_f is final concentration of each chemicals.

Density functional theory (DFT) calculation

We have employed the VASP to perform all the spin-polarized DFT calculations within the generalized gradient approximation (GGA) using the Perdew-Burke-Ernzerhof (PBE)formulation. We have chosen the projected augmented wave (PAW) potentials to describe the ionic cores and take valence electrons into account using a plane wave basis set with a kinetic energy cutoff of 400eV. Partial occupancies of the Kohn−Sham orbitals were allowed using the Gaussian smearing method and a width of 0.05 eV. The electronic energy was considered self-consistent when the energy change was smaller than 10−6 eV. A geometry optimization was considered convergent when the force change was smaller than -0.05 eV/Å2. Grimme's DFT-D3 methodology was used to describe the dispersion interactions among all the atoms. This slab was separated by a 15 Å vacuum layer in the z direction between the slab and its periodic images. During structural optimizations of the surface models, a 2×2×1 gamma-point centered k-point grid for Brillouin zone was used.

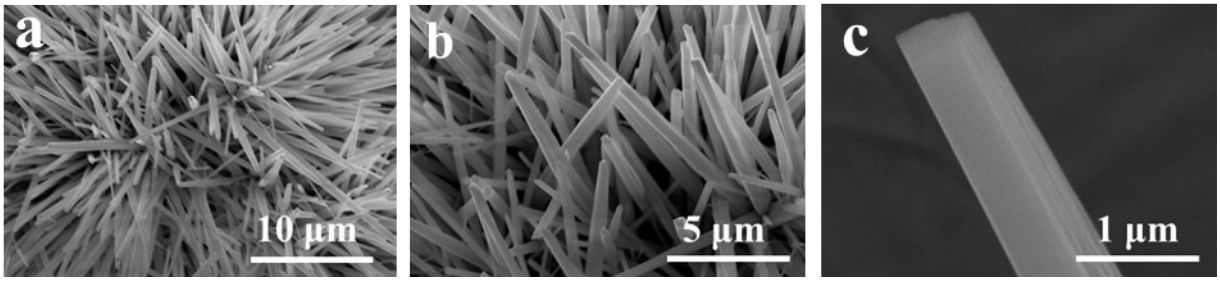

Figure S1 (a-c) SEM images of $NiMoO_4$/NF.

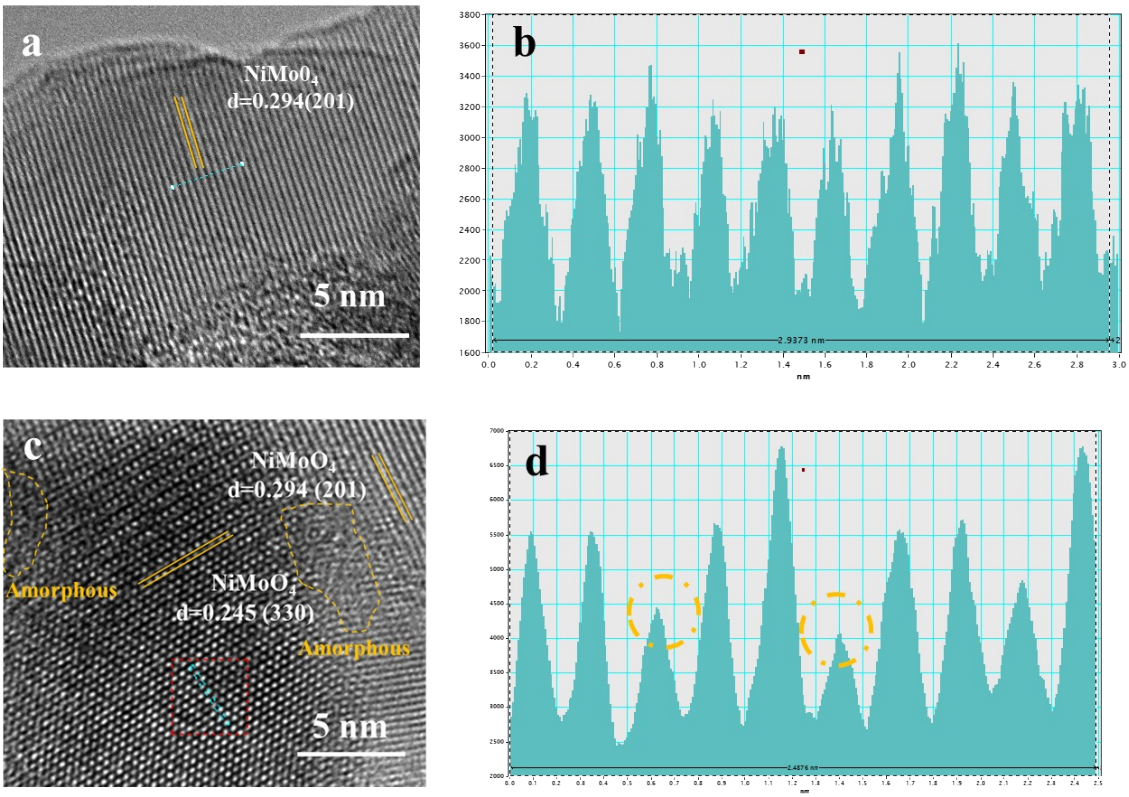

Figure S2 (a) TEM images of S/Dy–$NiMoO_4$/NF and (b) the line profiles extracted from the areas marked with blue rectangle in TEM image. (c) TEM images of Sv/Dy–$NiMoO_4$/NF and (d) the line profiles extracted from the areas marked with blue rectangle in TEM image.

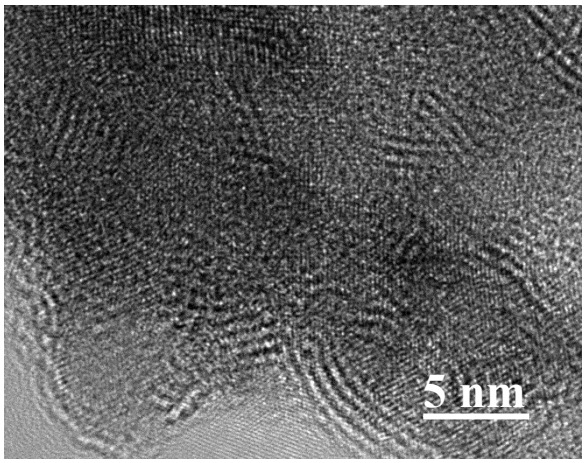

Figure S3. TEM images of Sv/Dy–$NiMoO_4$/NF.

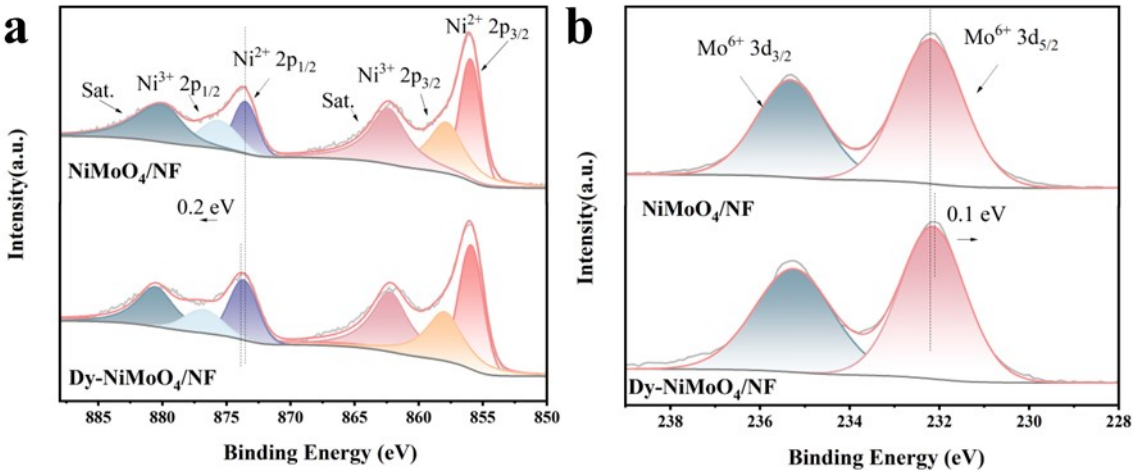

Figure S4 (a) High-resolution of Ni 2p spectra, (b) Mo 3d spectra in $NiMoO_4$/NF and Dy–$NiMoO_4$/NF

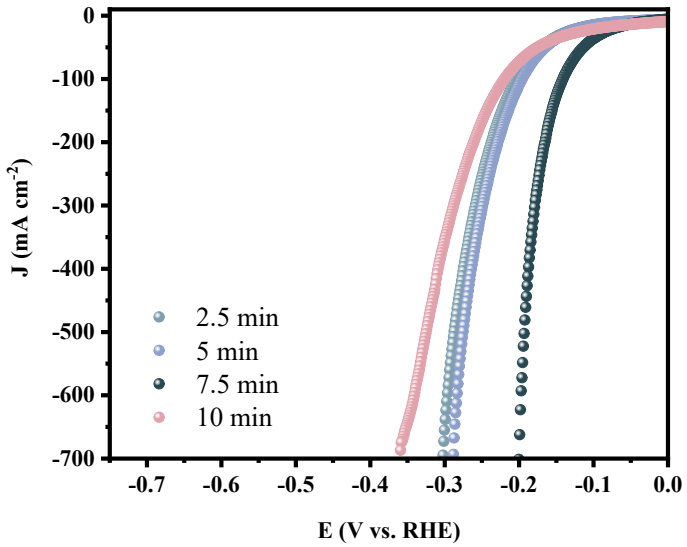

Figure S5 LSVs of Sv/Dy–$NiMoO_4$/NF for catalyzing HER at a scanning rate of 5 mV s^{-1} in 1 M KOH in three-electrode system with different etching time of Ar plasma.

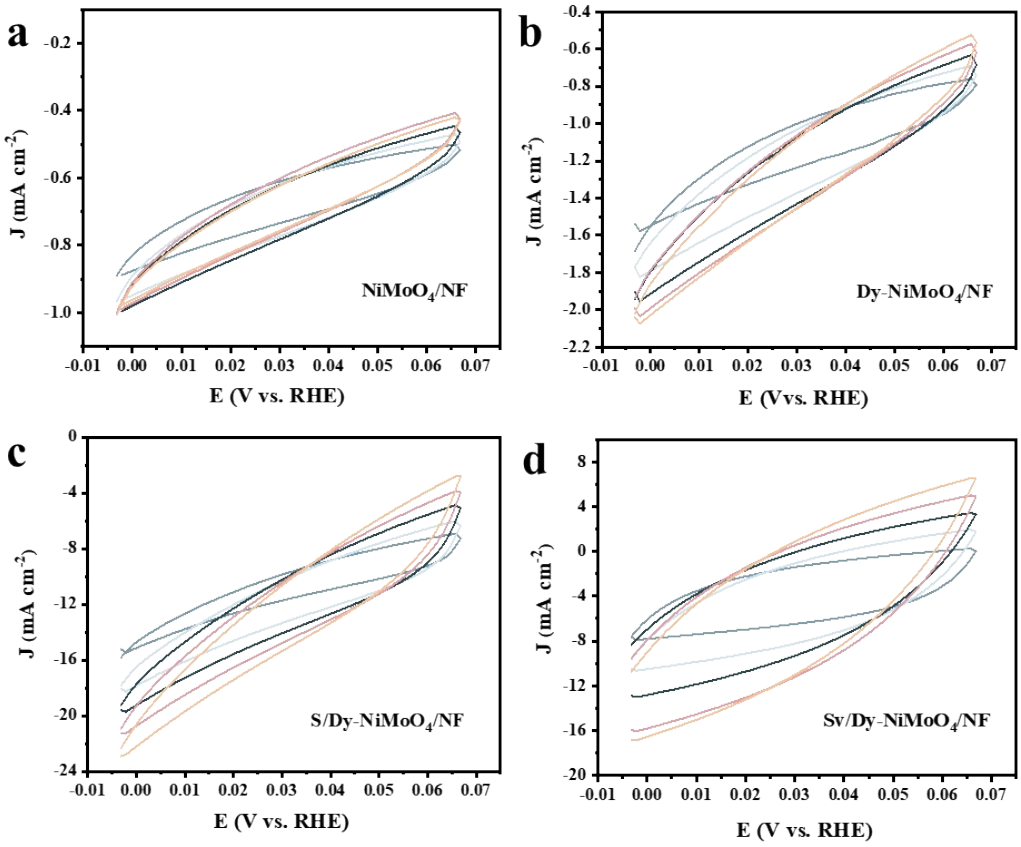

Figure S6 CV curves of (a) $NiMoO_4$/NF, (b) Dy–$NiMoO_4$/NF, (c) S/Dy–$NiMoO_4$/NF and (d) Sv/Dy–$NiMoO_4$/NF with the scan rates from 10 mV/s - 50 mV/s.

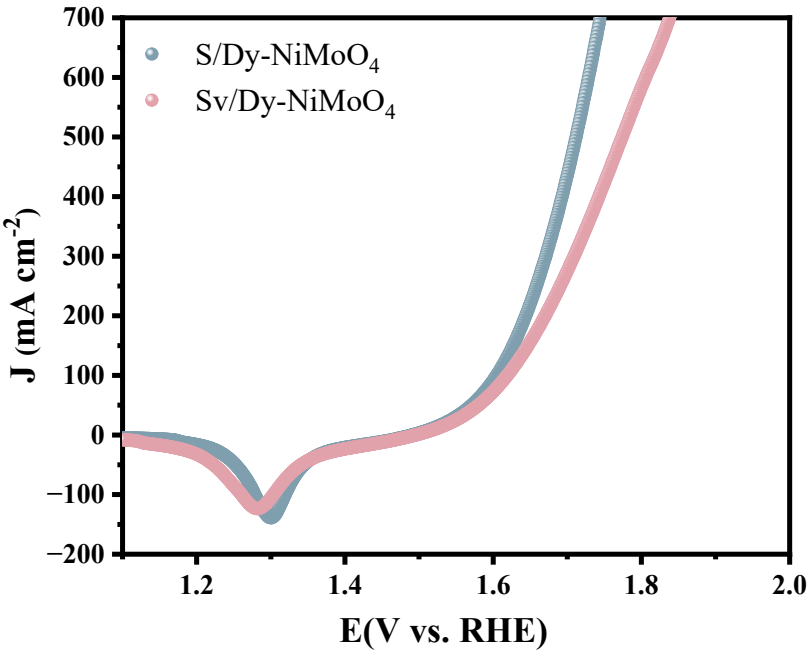

Figure S7 LSVs of the S/Dy–$NiMoO_4$/NF and Sv/Dy–$NiMoO_4$/NF for OER.

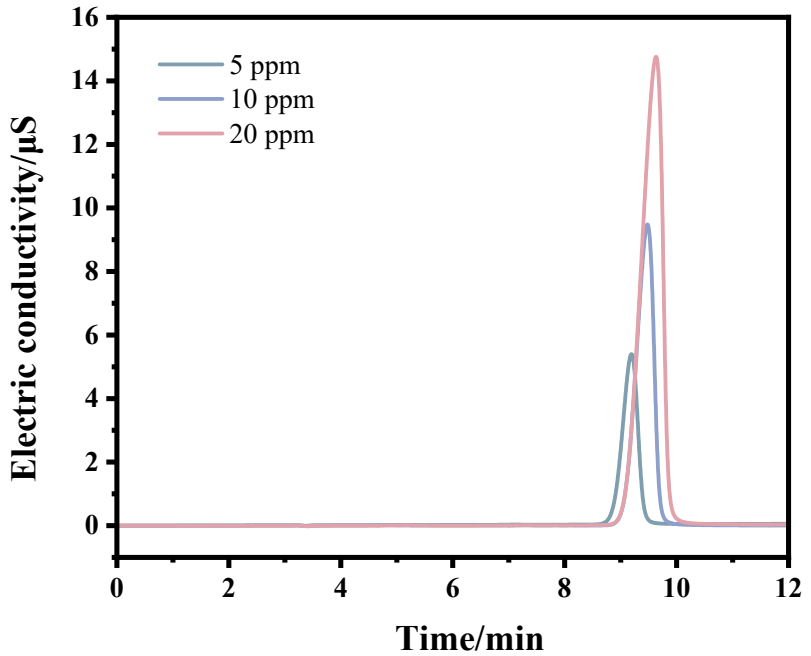

Figure S8 Standard IC chromatograms and the corresponding calibration curves of formate.

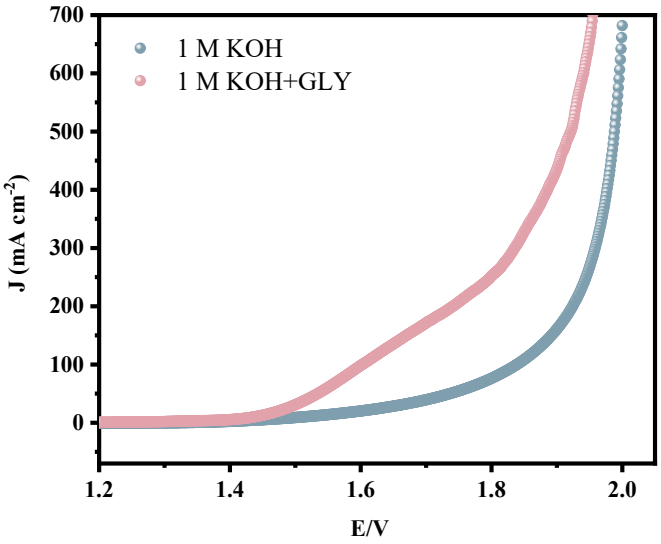

Figure S9 LSVs of the Sv/Dy–$NiMoO_4$/NF for overall water splitting and GOR.

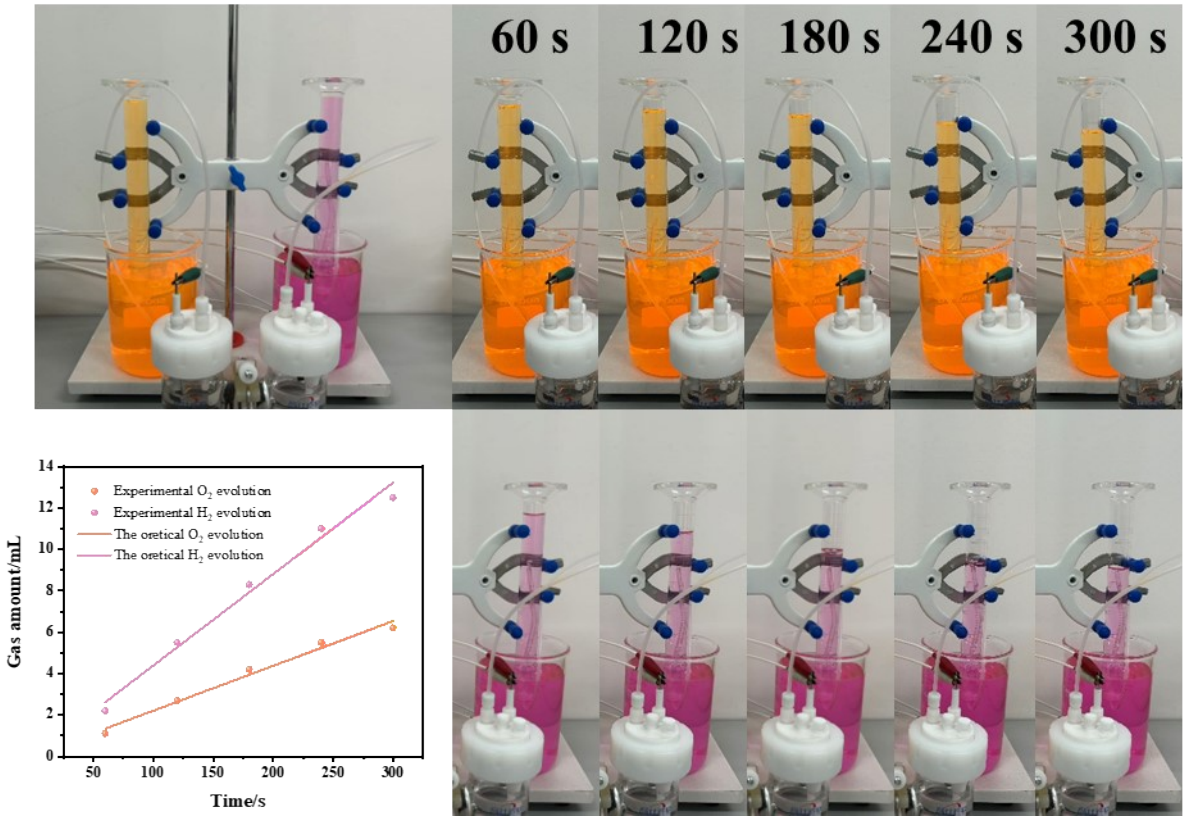

Figure S10 The amount of H_2 and O_2 varying with time based on overall water electrolysis system.

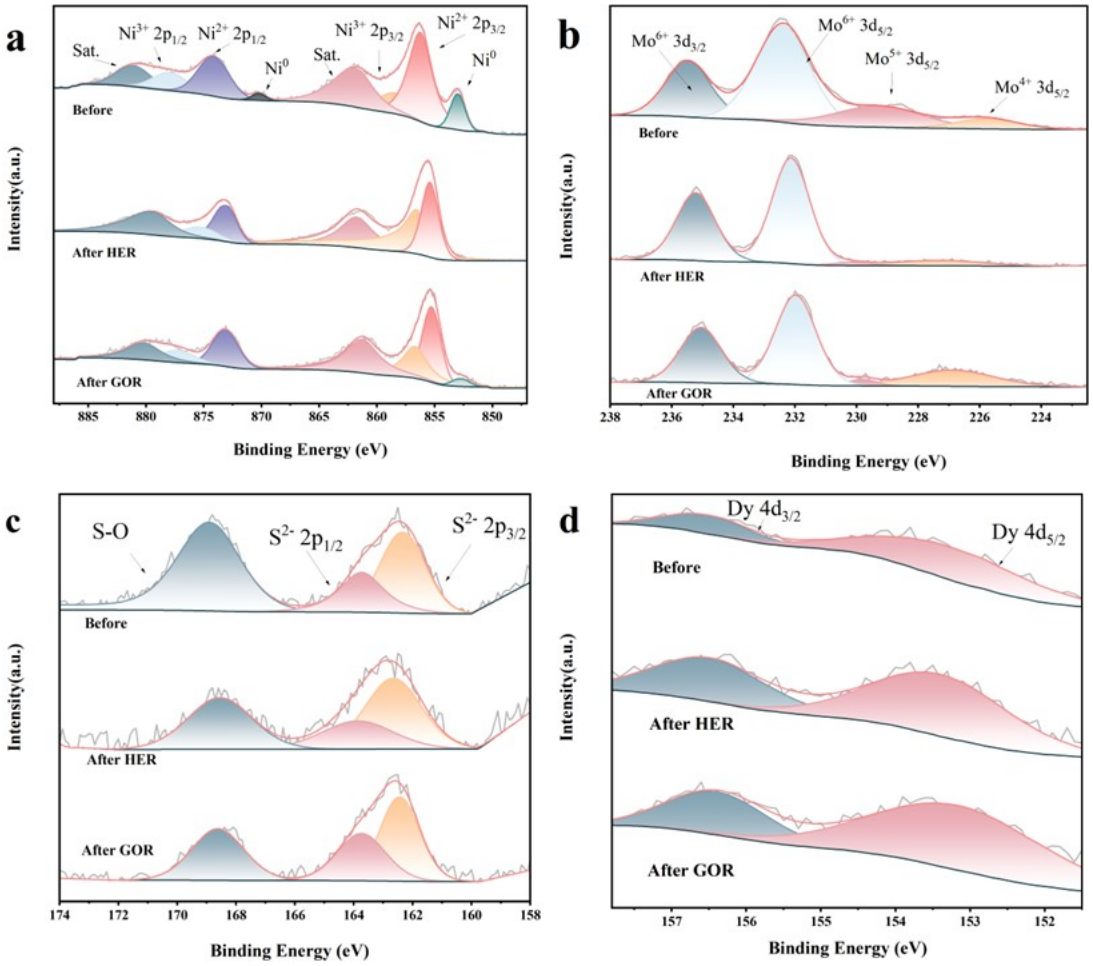

Figure S11 High-resolution of (a) Ni 2p spectra, (b) Mo 3d spectra, (c) S 2p spectra and (d) Dy 4d spectra in Sv/Dy–$NiMoO_4$/NF after HER and GOR.

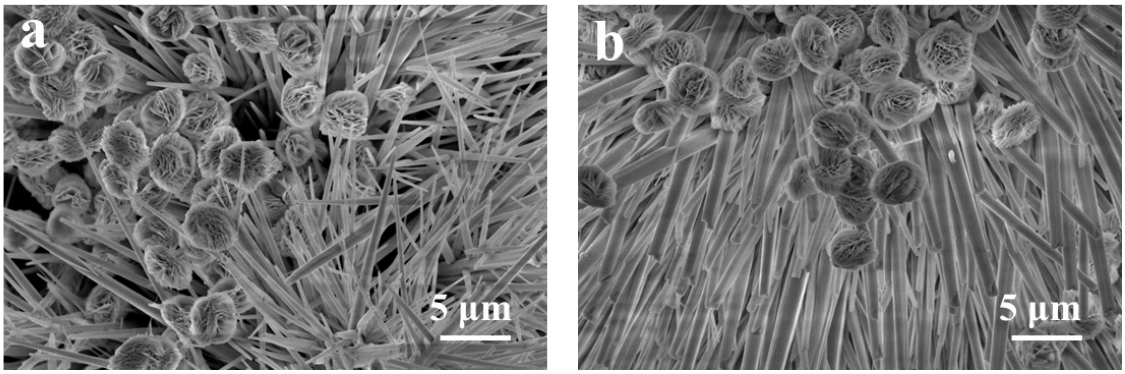

Figure S12 SEM images of Sv/Dy–$NiMoO_4$/NF after (a) HER and (b) GOR.

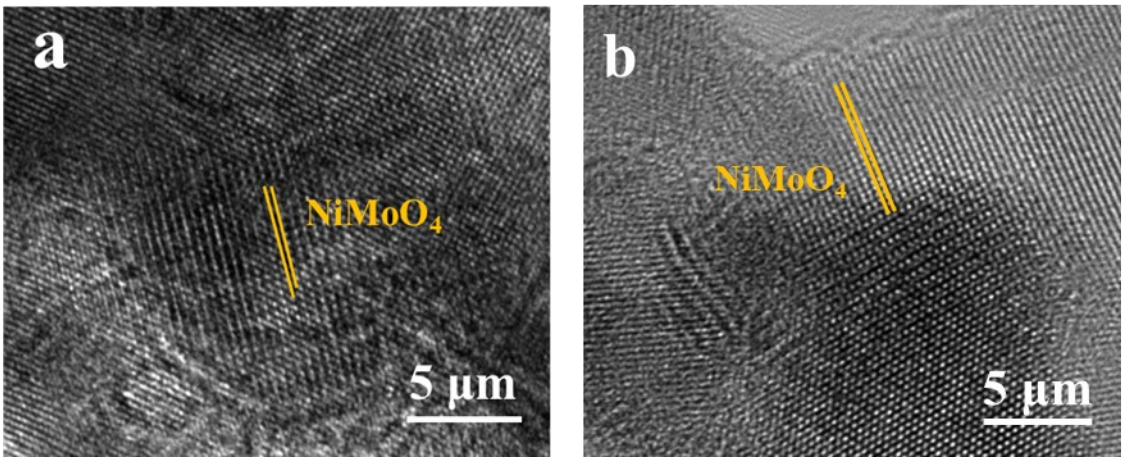

Figure S13 (a, b) TEM images of Sv/Dy–$NiMoO_4$/NF after (a) HER and (b) GOR.

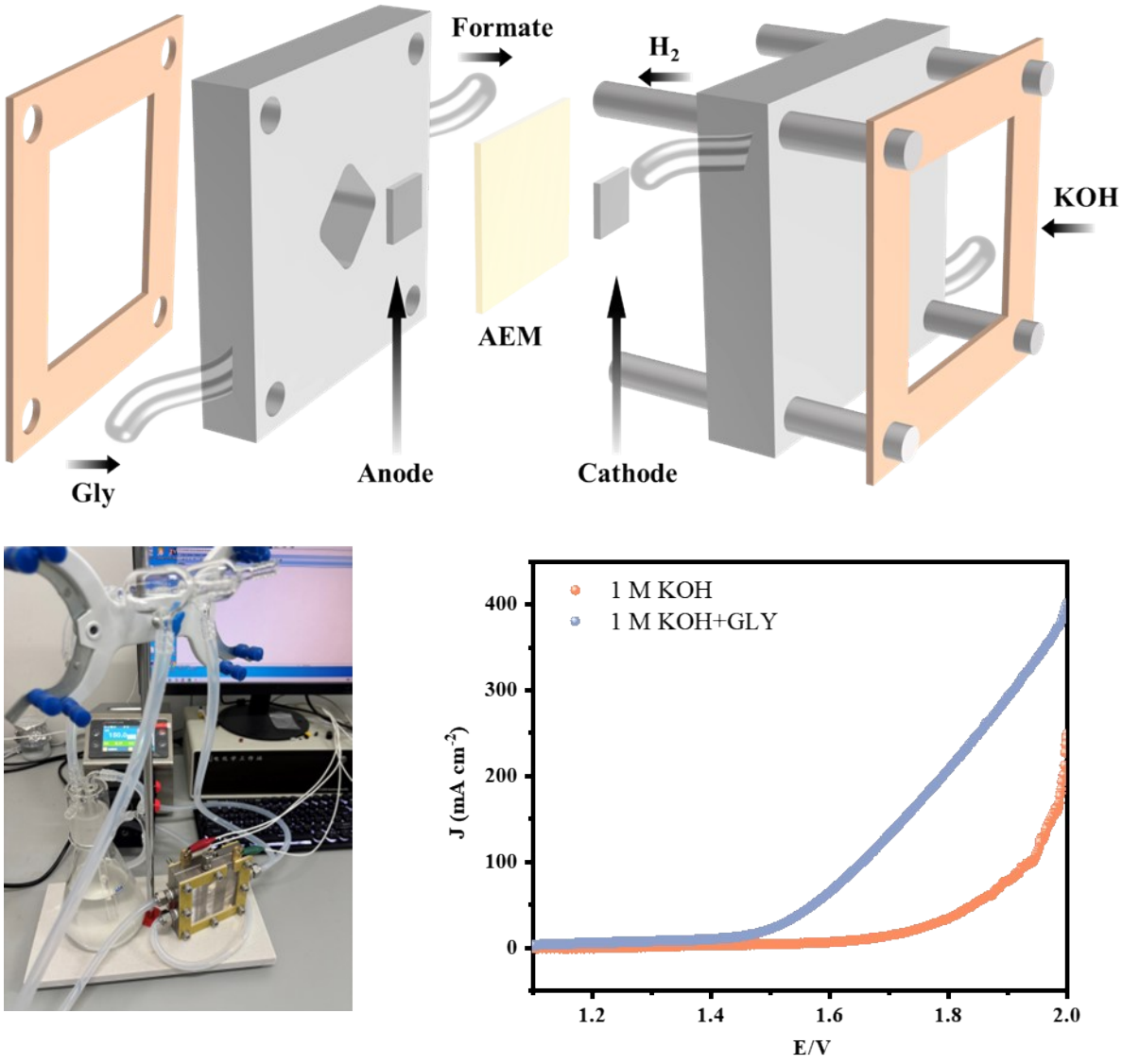

Figure S14 Schematic diagram of the AEM electrolyze and polarizationof the AEM electrolyzer using Sv/Dy–$NiMoO_4$/NF.

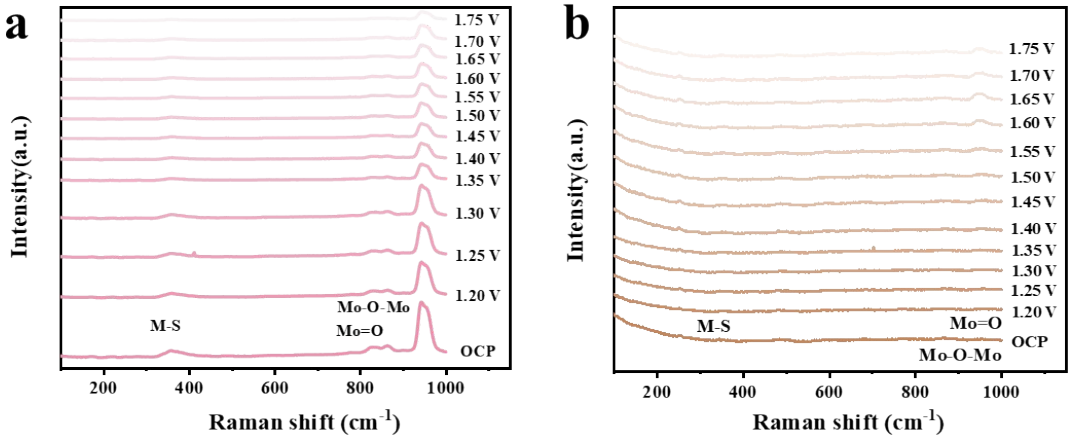

Figure S15 (a) In situ Raman spectra of Sv/Dy–$NiMoO_4$/NF electrode at various potentials in 1.0 M KOH and (b) 1.0 M KOH with 0.1 M Gly.

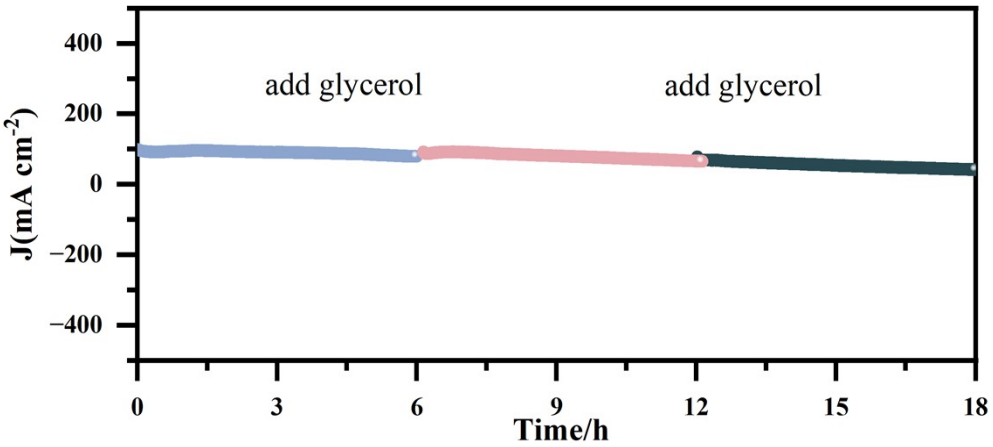

Figure S16 Chronoamperometry i-t curve of 18 h for GOR in three-electrode system.

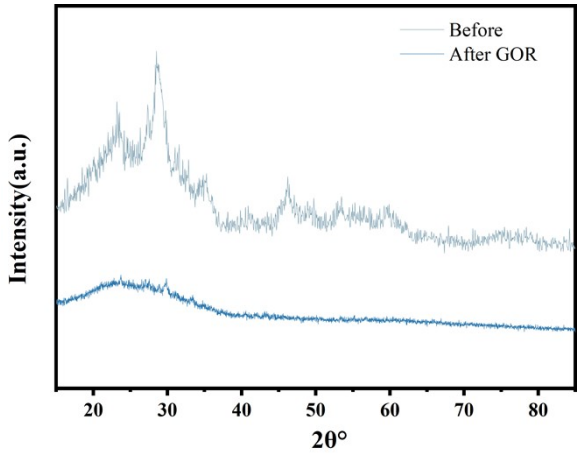

Figure S17 XRD patterns of Sv/Dy–$NiMoO_4$/NF before and after GOR.

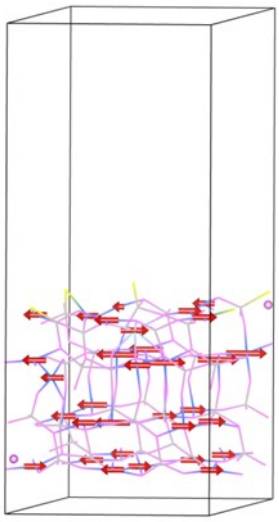

Figure S18 The magnetic moments (the arrows indicates the direction and magnitude) for Ni with both doping and vacancy (Model III)

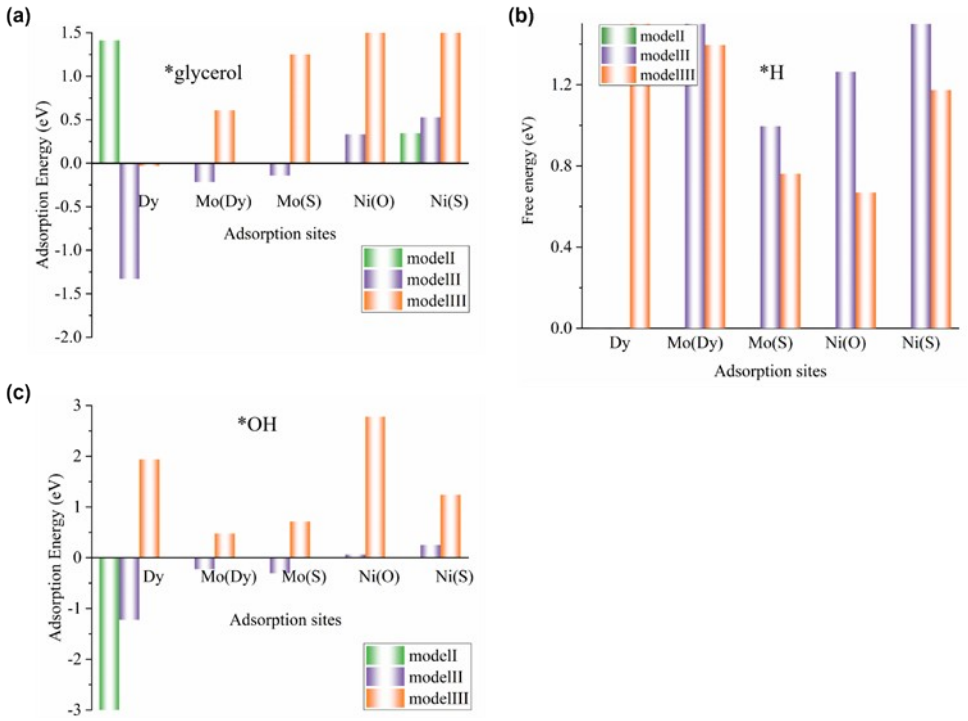

Figure S19 Adsorption energy of (a) *glycerol, (b) *OH and (c) *H on Model I, Model II and Model III from GGA+U calculations.

Table S1 Electrocatalytic HER activity of Ni-based catalysts

Catalysts	η10 / mV	Tafel / mV dec^{-1}	Electrolyte	Reaction type	Ref.
NiMoB	31	73.0	1 M KOH	HER	[1]
Ni-W-P/Mo	74	77.0	1 M KOH	HER	[2]
NC/NiO-Mo/NF	56	67.9	1 M KOH	HER	[3]
NiCoRux/SP	59	53.0	1 M KOH	HER	[4]
Ru-$NiMoO_4$-Vo/NF	49	49.6	1 M KOH	HER	[5]
NiCoP/P-MoS_2/CC	52.6	83.6	1 M KOH	HER	[6]
Mo-Ni_3S_2/Ni-N-C	71	53.0	1 M KOH	HER	[7]
$NiMoO_4$-S	105	84.1	1 M KOH	HER	[8]
Sv/Dy–$NiMoO_4$/NF	29	36.7	1 M KOH	HER	This work

Table S2 Electrocatalytic GOR activity of Ni-based catalysts

Catalysts	η10 / V	Electrolyte	Reaction type	Ref.
NC/Ni-Mo-N/NF	1.38	1 M KOH +0.1 M glycerol	GOR	[9]
Ni/P clusters	1.37	1 M KOH +0.1 M glycerol	GOR	[10]
$NiSe_2$ NPs	1.38	1 M KOH +0.1 M glycerol	GOR	[11]
Ni_3N-$Ni_{0.2}Mo_{0.8}N$	1.40	1 M KOH +0.1 M glycerol	GOR	[12]
NiCrO-$V_{Cr,O}$	1.37	1 M KOH +0.1 M glycerol	GOR	[13]
Sv/Dy–$NiMoO_4$/NF	1.34	1 M KOH +0.1 M glycerol	GOR	This work

Reference:

[1] C. Pang, W. Xu, Y. Liang, Z. Li, S. Wu, Z. Cui, H. Sun, H. Jiang, S. Zhu, Improved hydrogen evolution performance of Ni-based nanoporous catalyst with Mo and B co-addition, *J Colloid Interf Sci*, 2024, **656**, 262-269.

[2] Q Kong, Y Li, H Ma, Q Zhao, L Yang, R Xu, H Guo, Electrochemical synthesis of Ni-W-P/Mo electrode for highly efficient and stable hydrogen evolution reaction, *Ind Eng Chem Res*, 2025, **64**, 1173-1180.

[3] B Qiu, D Zhang, R Fang, Y Wang, B Shen, J Dai, H Chu, In situ synthesis of Ni, Mo bimetallic crystalline-amorphous co-existing heterostructures for efficient hydrogen evolution reaction, *Compos Part B-Eng*, 2025, **307**, 112956.

[4] L Li, H Qiu, Y Zhu, G Chen, S She, X Guo, H Li, T Liu, Z Lin, H Zhou, Y Zhu, M Yang, B Xu, H Huang, Atomic ruthenium modification of nickel-cobalt alloy for enhanced alkaline hydrogen evolution, *Appl Catal B-Environ Energy*, 2023, **331**, 122710.

[5] D Sui, R Luo, S Xie, H Zhang, T Ma, H Sun, TT Jia, J Sun, X Li, Atomic ruthenium doping in collaboration with oxygen vacancy engineering boosts the hydrogen evolution reaction by optimizing H absorption, *Chem Eng J*, 2024, **480**, 148007.

[6] Q Luo, Y Lv, P Zhang, Z Zhao, X Bao, L Gou, H Luo, X Fan, F Ma, Interface engineering of hollow Janus-structured NiCoP/P-MoS_2 heterojunction as self-supported electrode enables boosted alkaline hydrogen evolution reaction, *J Colloid Interf Sci*, 2025, **684**, 668-677.

[7] C Zhang, J Cheng, F Yang, Y Sun, X Sun, K Wei, G Ma, J An, M Zhao, J Liu, Y Li, Optimizing hydrogen adsorption via Mo-doped Ni_3S_2 nanoparticles anchored on Ni−N−C framework as an efficent electrocatalyst for all-pH hydrogen evolution, *Int J Hydrogen Energ*, 2025, **166**, 151007.

[8] HMCM Jayawardana, S Meng, BA Yusuf, J Jing, H Ren, Q Nie, J Xie, M Chen, Y Xu, Synergistic flower-like N-doped Co/Mo_2C catalyst for hydrogen evolution reaction in universal pH and high-performance alkaline water-splitting, *Mater Today Chem*, 2025, **43**, 102476.

[9] Y Xu, M Liu, S Wang, K Ren, M Wang, Z Wang, X Li, L Wang, H Wang, Integrating electrocatalytic hydrogen generation with selective oxidation of glycerol to formate over bifunctional nitrogen-doped carbon coated nickel-molybdenum-nitrogen nanowire arrays, *Applied Catalysis B: Environmental*, 2021, **298**, 120493.

[10] R Deng, Z Wang, Y Xie, X Wu, K Ma, B Liu, X Qin, H Shu, F Mo, Y Li, H Yang, W Yu, Y Hu, J Chen, W Liu, Ni/P clusters perform as a reaction switch dispersed on co-based electrocatalyst for glycerol oxidation coupling with alkaline hydrogen production, *Inorg Chem Commun,* 2024, **167**, 112687.

[11] L Yang, Y Ma, J Yu, J Arbiol, J Li, A Cabot, Organic oxidation-assisted hydrogen production: glycerol electroreforming to formate on nickel diselenide nanoparticles, *J Colloid Interf Sci*, 2025, **700**, 138535.

[12] X Liu, Z Fang, X Teng, Y Niu, S Gong, W Chen, TJ Meyer, Z Chen, Paired formate and H_2 productions via efficient bifunctional Ni-Mo nitride nanowire electrocatalysts, *J Energy Chem,* 2022, **72**, 432-441.

[13] LX Chen, ZW Chen, Y Zhang, CC Yang, Q Jiang, Insight into the excellent catalytic activity of (CoMo)S_2/graphene for hydrogen evolution reaction, *Appl Catal B-Environ Energy*, 2019, **258**, 118012.